Sensors and Materials, Vol. 17, No. 5 (2005) 277–288
MYU Tokyo

S & M 0606

Mechanical Characterization of Gold Thin Films Based on Strip Bending and Nanoindentation Test for MEMS/NEMS Applications

Chang-Wook Baek*, Jong-Man Kim[1], Yong-Kweon Kim[1]
Jae Hyun Kim[2], Hak Joo Lee[2] and Seung Woo Han[2]

School of Electrical and Electronics Engineering, Chung-Ang University
221 Heuk-Seok Dong, Dong-Jak Gu, Seoul 156-756, Korea
[1]School of Electrical Engineering and Computer Science, Seoul National University
301-1118 (#007) Kwanak P. O. Box 34, Seoul 151-600, Korea
[2]Micro System and Structural Mechanics Group, Korea Institute of Machinery and Materials
171 Jang-dong, Yuseong-Gu, Daejeon 305-343, Korea

(Received August 24, 2004 ; accepted December 4, 2004)

Key words: MEMS, NEMS, gold thin film, mechanical properties, strip bending test, nanoindentation test

In this paper, we report the mechanical properties of micro/nanometer-thin gold films evaluated by a strip bending technique and a conventional nanoindentation test for micro-nano-electromechanical systems (MEMS/NEMS) applications. Nanometer-thin freestanding fixed-fixed gold strip specimens with different thicknesses of 200, 500 and 1000 nm have been prepared to observe the effect of size dependence on the mechanical properties. All the specimens are fabricated over the open window in silicon wafers using the metal lift-off and silicon deep etching processes. A strip bending test has been performed on the fabricated freestanding strip specimens using a commercial nanoindenter with a wedge-type indenter tip for applying a line load to the strip. A nanoindentation test has also been performed on the same gold films fixed on the silicon substrate using a nanoindenter with a continuous stiffness measurement (CSM) option. Experimental details of the strip bending test and the measured mechanical properties are introduced. In addition, the results are analyzed to validate the two measurement techniques.

1. Introduction

As a key factor for micro-nano-electromechanical systems (MEMS/NEMS) applications, micro/nanometer-thin film structures have been widely used. Their mechanical properties are essential in the design step of MEMS/NEMS devices since they are known to be different from those of bulk material and exhibit a dependence on the specimen size.[1–5]

Recent developments in micromachining technology have enabled us to fabricate and

*Corresponding author, e-mail address: cwbaek@cau.ac.kr

control mechanical structures on the scale of micro/nanometers. This presents a whole new spectrum of opportunities to build MEMS/NEMS devices and at the same time brings problems of material behavior on the micro/nanoscale into the domain of engineering. A precise characterization of the mechanical properties of these structures is required in order to use them as structural/functional elements in the MEMS/NEMS devices.[2] Currently, many potential applications, such as high-frequency resonators and ultrasensitive force sensors utilizing advantages of nanoscale structures, are being proposed and investigated. However, they are not really practical because mechanical properties of nanoscale structures have not been well explored. The current concept and software developed for designing nanostructures are based on bulk material properties without considering of the size-dependent phenomenon. This limits the further development and application of micro/nanomechanical structures and devices.[1]

During the past years, several test methods have been employed to measure the mechanical properties of micro/nanometer-thin films, such as the nanoindentation test, microtensile test, and so forth.[6,7] The nanoindentation test, which is a common technique for investigating material properties, can be used to measure the elastic modulus and hardness of materials by impressing a specially designed indenter onto the material. Nanoindentation has a simple test procedure and the sample preparation for this test is relatively easy. It is known, however, that the method requires several assumptions and models to extract the material properties from the measured data, and the result contains the substrate effect, both of which may lead to an inaccurate evaluation. In the microtensile test, the quantitative analysis of material is possible, but it requires precise testing technologies and has difficulties in preparing the test specimen.

In this study, we focus on the strip bending technique to measure the mechanical properties of thin films for MEMS/NEMS applications. The strip bending test is performed by applying an external load to the fixed-fixed strip specimen with a nanoindenter and analyzing the resulting load-displacement characteristics. Using this method, we can obtain tensile properties of thin films just as in the microtensile test, while maintaining simplicities in fabrication, alignment, and fixing of the specimens. In this paper, techniques and methodologies of the strip bending test are described in detail. To validate the procedure, nanometer-thin freestanding gold strip specimens have been fabricated by micromachining and tested using the established strip bending method. The results from the strip bending test along with those from the nanoindentation test using a continuous stiffness measurement (CSM) technique are introduced and compared.

2. Strip Bending Test

In the strip bending test, load-displacement characteristics of a fixed strip specimen are used to evaluate the mechanical properties of materials. The term "strip specimen" used in this study, like a membrane, represents a type of beam structure that has a very small thickness with respect to its surface area and therefore cannot support a bending moment. The strip specimen, however, should be distinguished from the membrane structure in the aspects that it exhibits a simplified 2-dimensional deformation behavior since its width is much smaller than its length.

Basic concepts of the strip bending test are illustrated in Fig. 1. A vertical line load generated from the magnetic actuator of the nanoindenter system is applied at the center of a strip specimen through the indenter tip, as shown in Fig. 1(a). At the same time, the displacement of the specimen is sensed with a capacitive displacement gauge of the nanoindenter. Load and displacement responses of the specimen are stored in the control PC and analyzed.

The load-displacement relationship obtained from this test is analyzed under the following three assumptions: (1) The strip specimen shows isotropic, linear, elastic behaviors, (2) The strip specimen can support only a tension along its length, not a bending moment, and (3) The deformation in the lateral direction can be simplified under the plane-strain condition. With these assumptions, the relationship between the load and the displacement is given by

$$P = 2\sin\theta\left(\sigma_0 + \frac{1-\cos\theta}{\cos\theta}E\right)Wt, \tag{1}$$

where P is the vertical indenter load applied to the specimen, θ is the angle of deflection, E is the elastic modulus, and $2L$, W and t are the length, width and thickness of the strip specimen, respectively, as shown in Fig. 1(b). In eq. (1), $\tan\theta = \delta / L$, where δ is the

(a)

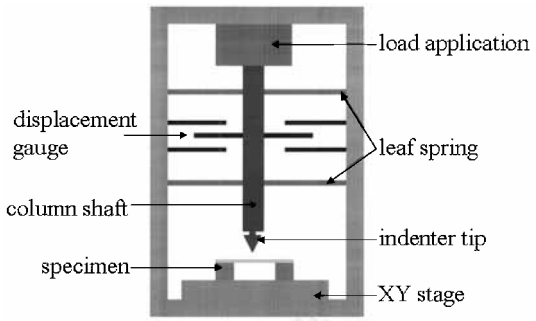

(b)

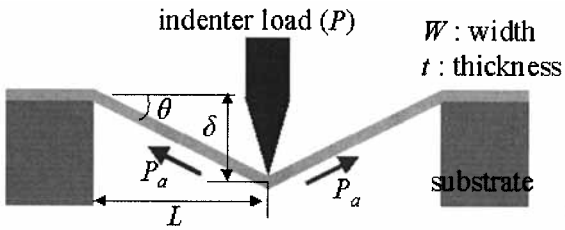

Fig. 1. (a) Schematic representation of the strip bending test using a nanoindenter system. (b) Side view diagram of the freestanding strip specimen loaded by nanoindenter.

displacement at the center of the specimen (loading point), and σ_0 is the initial stress existing in the freestanding strip specimen before the external load is applied. If the displacement of the specimen is sufficiently small, the angle θ can be approximated as $\theta \cong \delta / L$. Then eq. (1) is modified as

$$P = 2\frac{\delta}{L}\left[\sigma_0 + \frac{1}{2}\left(\frac{\delta}{L}\right)^2 E\right]Wt. \tag{2}$$

From the strip bending test, we can obtain the load-displacement curve of a strip specimen, and this curve is subsequently converted into the stress-strain curve by the simple method that will be described in the following section. We can evaluate the elastic modulus and initial stress of the specimen using eq. (1) or (2), and the yield and tensile (fracture) stress from the stress-strain curve.

3. Experimental Details

3.1 *Specimen design*

As mentioned earlier, the strip specimen is defined as a structure that cannot support a bending moment. Some factors should be considered in the design of a specimen shape to satisfy this condition. The maximum displacement of the specimen must be much larger than its thickness (normally 10 times larger). In addition, the length of the strip specimen should be designed larger than the displacement during the loading step to keep the specimen in its elastic region as the displacement gradually increases. If we assume that the strain at a yield point is about 0.4%, the length of the beam should be at least 12 times larger than the maximum displacement. The dimensions of the specimens were determined based on these considerations. Three different specimen thicknesses of 200, 500 and 1000 nm were used to investigate the size effect according to the thickness variations. The length of the specimen was set to be 400 μm based on the assumption of a maximum elastic displacement of about 30 μm. The width of the specimen was set to be 10 μm, which is at least 10 times larger than the maximum specimen thickness used.

3.2 *Specimen fabrication*

Freestanding fixed-fixed gold strip specimens for the strip bending test were fabricated by micromachining. In the design of the fabrication process, three major points for accurate measurements were considered: (1) A relatively large space is required underneath the test beam structures so that we can apply a mechanical load sufficiently large enough to break the beam, (2) The undercut of the substrate around the anchor region should be minimized to reduce the measurement errors caused by the ambiguous definition of the specimen length, and (3) The test structural material obtained after deposition should not be damaged by subsequent fabrication processes. For these reasons, we used protective layers for the passivation of the structure and through-wafer silicon DRIE to fully remove the substrate under the specimen.

The fabrication process for the strip specimen is shown in Fig. 2. The process begins with the deposition of a 500-nm-thick PECVD oxide layer on a 520-μm-thick silicon (100) wafer (Fig. 2(a)). This oxide layer protects the structural gold layer during the through-wafer silicon DRIE from the back for release like an etch-stop layer. On this wafer, a negative-tone photoresist (AZ 5214E) is patterned to form a lift-off mold for gold patterning. Then a Cr (3 nm)/Au (200, 500, or 1000 nm) bilayer is deposited by thermal evaporation. Here, a very thin Cr layer is used to enhance the adhesion of gold to the substrate.The evaporation process of the material is performed at room temperature; no forced heating using an external heater is performed. The change in the substrate temperature due to the Joule heating from the boat is monitored using the thermocouple placed right behind the substrate. The maximum substrate temperature during the evaporation process is only 30–35°C, even for a 1000-nm-thick film that requires the longest deposition time. Hence, the thermally induced stress effect is negligible. The gold layer is patterned into the strip shape by the lift-off technique (Fig. 2(b)). Another 500-nm-thick oxide layer is deposited again onto the surface of the gold structure by PECVD (Fig. 2(c)). This top oxide layer prevents the surface of a gold beam from being damaged by the plasma

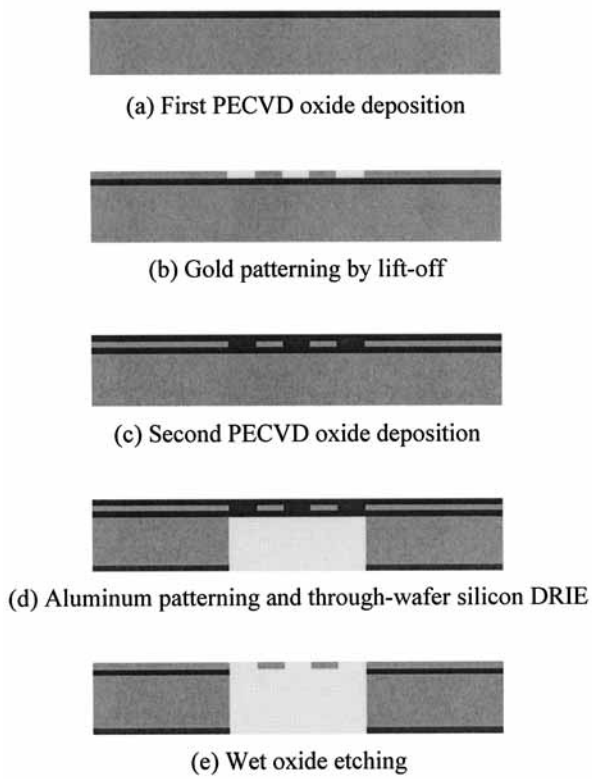

Fig. 2. Fabrication process of the freestanding gold strip specimen.

during the silicon DRIE process. To release the gold structure, a 500-nm-thick aluminum hard mask is evaporated and patterned by the lift-off technique on the back of the wafer, and the silicon wafer is etched to the first oxide layer using an ICP silicon deep etcher (Fig. 2(d)). At this stage, a freestanding oxide-gold-oxide layer is obtained. The protective oxide layers are removed using a 7:1 buffered oxide etchant (BOE). Finally, the samples are rinsed in DI water and IPA, and then dried in oven to obtain freestanding gold strip specimens (Fig. 2(e)).

Using this process, we successfully fabricated the freestanding thin gold strip specimens over the open windows in silicon substrates. SEM images of the fabricated gold strip specimens are shown in Fig. 3. Under the SEM observation, the specimens with thicknesses of 200 and 500 nm seem to be flat without deformation or buckling as shown in Fig. 3(a), but the 1000-nm-thick specimens are deformed downward due to the compressive stress in the strip. In the SEM image shown in Fig. 3(b), we can see that the sidewall of the etched silicon is vertical and there is no undercut of the substrate along the longitudinal direction.

3.3 *Testing procedure*

The testing equipment setup for the strip bending test is similar to that developed by Espinosa *et al.*[3,5] Strip bending tests are performed with a commercial nanoindenter XP of MTS Corp. The displacement and load resolutions of the nanoindenter XP are 0.01 nm and 50 nN, respectively. The specimens are fixed to the sample holder using an adhesive and located under the nanoindenter head. A wedge-type indenter tip is mounted on the indenter head to apply a line contact load. The indenter tip is moved at a constant speed of 50 nm/s to the sample, and at the same time, the load-displacement signal is recorded. We performed strip bending tests to at least three different specimens for each film thickness.

Measured data from the above steps are not exactly the same as the actual data of the specimen, since they contain several unexpected effects such as the ambiguity of the

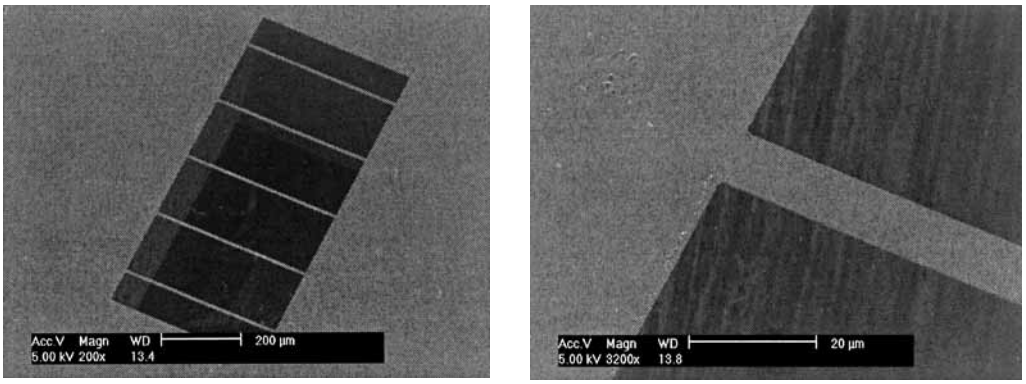

(a) (b)

Fig. 3. SEM images of the fabricated gold strip specimens: (a) Perspective view of a 200-nm-thick specimen. (b) Enlarged view near the fixed anchor region of (a).

surface location due to the low stiffness of the strip, thermal drift, and stiffness of the leaf spring of the indenter. Therefore, we should carry out data correction by taking several conversion steps. For the precise detection of the surface position, we make three successive indents on the two anchor regions and the center of the strip. The average of the first two positions is used as a surface location. The stiffness of the leaf spring is compensated by subtracting the load-displacement data without a specimen (air data) from the data with a specimen. Thermal drift error is also considered based on the linear approximation of a thermal fluctuation. A typical load-displacement curve for a 200-nm-thick strip specimen, after all of the compensation steps are processed, is shown in Fig. 4.

The measured load-displacement curve can be converted into the stress-strain curve by referring to the geometrical relationships in Fig. 1(b). The actual (tensile) load in the plane of the strip specimen P_a is calculated from the applied indenter load P,

$$P_a = \frac{P}{2\sin\theta}. \tag{3}$$

Then, the stress in the membrane is given by

$$\sigma = \frac{P_a}{A} = \frac{P}{2Wt\sin\theta} \tag{4}$$

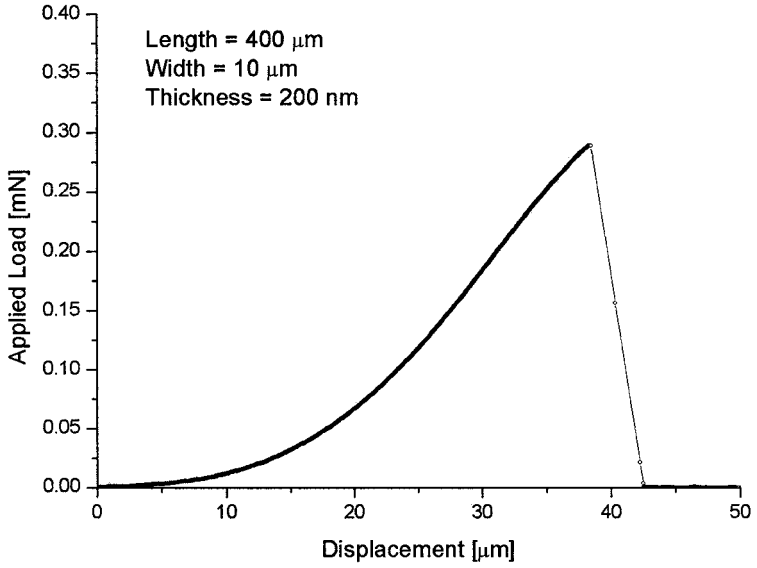

Fig. 4. A typical, completely compensated load-displacement curve measured for a 200-nm-thick gold strip specimen.

and the strain is calculated by

$$\varepsilon = \frac{\sqrt{L_2 + \delta^2}}{L} - 1. \tag{5}$$

4. Results and Discussions

4.1 *Strip bending test results*

Stress-strain curves measured for strip specimens of different thicknesses are shown in Fig. 5. It is likely that the specimens with the same thickness show almost similar behaviors except for some differences in failure stress and strain. Elastic modulus and the initial stress existing in the freestanding strip specimen can be calculated by the linear fitting of the stress-strain curve within its elastic region. Elastic modulus is the slope of the fitted line, and the initial stress is determined at the point of intersection of the fitted line with the vertical stress axis, as illustrated in Fig. 5(a). Other methods of obtaining these values are fitting the measured load-displacement data directly into eq. (1) and extracting the parameters. In this work, we used the latter method because the strain of eq. (5) was derived under the assumption of uniform strain over the entire strip specimen, which might be different from the real situation and therefore cause the measurement errors. Yield stress is determined at the intersection of the stress-strain curve and a 0.2% offset line having the slope of the elastic region. Tensile stress is defined as the maximum stress at the moment of specimen fracture.

The elastic modulus, initial stress, yield stress and tensile stress values measured for the specimens of different thicknesses are summarized in Table 1. These values are extracted independently for each specimen from either load-deflection or stress-strain curve.

Elastic modulus is measured differently from 27 to 37 GPa, but the results do not show any noticeable large deviations from sample to sample with respect to the different thicknesses. The measured value is significantly lower than the bulk modulus of gold (80 GPa). Compared with the previous works on micron-thick gold films (30-78 GPa [6,8]) and submicron-thick gold films (53–55 GPa[3,5]), the elastic modulus in our experiments are distributed in a lower range of the reported values. The method of Espinosa and Prorok [3,5] underestimates the strain along the test section of specimens because the strain along the entire length of the specimen is assumed to be uniform. This may possibly lead to the overestimation of the elastic modulus. The lower modulus values in our experiments are believed to be the result of the structural anisotropy caused by the preferred orientation of the film texture.[5]

The initial stress in the freestanding gold strip specimen was found to be tensile in the 200-nm-thick films while compressive in the 500 and 1000-nm-thick films. By SEM observation, we cannot differentiate the state of the initial stress between 200-and 500-nm-thick films since they are all flat. However, it is obvious that the 500- and 1000-nm-thick films are in compression from a flat, zero-stress region at the beginning of the stress-strain curve. In these specimens, the fitted line intersects with the negative part of the stress axis,

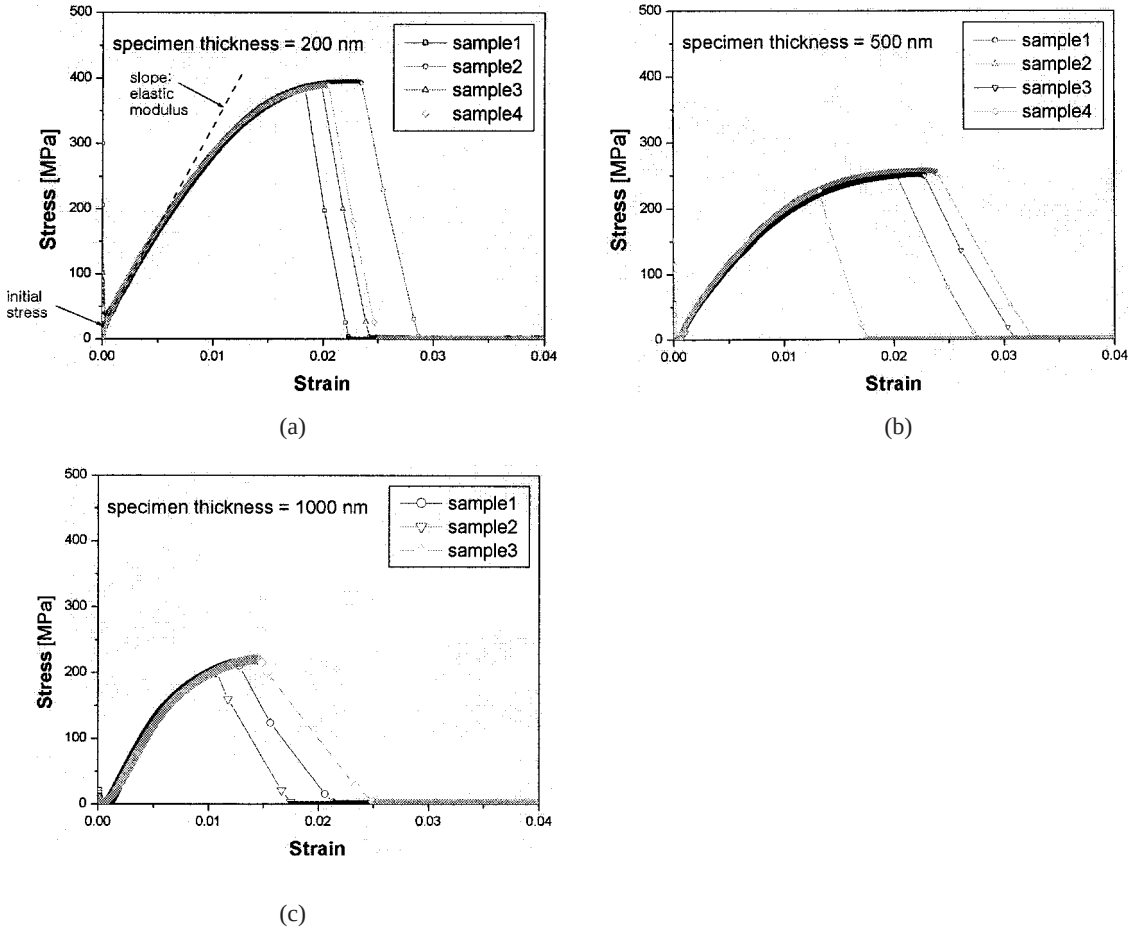

Fig. 5. Stress-strain curves for (a) 200- (b) 500- and (c) 1000-nm-thick gold films.

Table 1
Measured mechanical properties from the strip bending tests.

Thickness (nm)	Sample ID	Elastic modulus (GPa)	Initial stress (MPa)	Yield stress (MPa)	Tensile stress (MPa)
200	1	30.9	20.4	315	383
	2	30.7	20.4	319	395
	3	31.5	17.4	306	388
	4	36.6	12.4	265	390
500	1	34.0	–19.4	148	250
	2	32.5	–11.8	160	256
	3	32.6	–18.1	147	252
	4	33.0	–14.3	158	227
1000	1	33.7	–37.1	—	215
	2	32.1	–30.0	—	202
	3	26.7	–20.9	—	220

representing the compressive initial stress. The initial downward buckling deformation of the 1000-nm-thick films observed by SEM is another strong evidence of compressive stresses in those specimens. Note that the initial stress here is for the freestanding films after being released, and thus it may be different from the residual stress of the film deposited on the substrate. Initial stress is dependent on the strip and substrate geometry, elasticity of the substrate, etched window, residual stress, and even on the post-process conditions.[8] A sophisticated analysis is required to directly convert the initial stress into the film residual stress, and this topic will be dealt with in a separate paper. In the design of the MEMS/NEMS devices, initial stress is informative rather than the film residual stress since the device performance characteristics such as pull-in voltages and resonance frequencies are directly related to the initial stress.

Experimental results show that the yield and tensile stress of the film tend to increase as the thickness of the film decreases. In our experiments, the 200-nm-thick films exhibit the highest yield and tensile strength, which implies a brittle behavior of thinner films. The stress-strain curves of the 1000-nm-thick films have a relatively wide nonlinear region at the initial loading. This is mainly due to the misalignment of the indenter tip and the ambiguous initial displacement caused by the buckling deformation. Because of this nonlinear region, it is difficult to draw the 0.2% offset line exactly. For this reason, yield stress data of the 1000-nm-thick films are not shown in Table 1. Since the strength and plastic deformation behavior of thin films are strongly dependent on the film thickness, these mechanical parameters should be carefully evaluated using specimens that have the same thickness and experience the all fabrication processes.

4.2 *Nanoindentation test results*

Nanoindentation tests were also performed to measure the elastic modulus of gold thin films in the direction of a surface normal. The nanoindenter DCM of MTS Corp. with a CSM (continuous stiffness measurement) option was utilized to obtain the elastic modulus with varying indentation depth, and the conventional Oliver and Pharr's indentation theory[9] was used to interpret the measured indentation data. We ran 16 indents on each kind of sample, and the averages of the measured data are shown in Fig. 6 as a function of indentation depth. Measured results reveal that the elastic modulus increases with indentation depth, which denotes that there is a severe substrate effect in the measured data (Note that Oliver and Pharr's theory cannot take the substrate effect into account). A rule of thumb for extracting the elastic modulus of the film is to take the data from the region of indentation depth much smaller than the film thickness. In our experiment, we used the data from 2.5% to 5% of a film thickness as the elastic modulus of the films in order to eliminate both the scattering of data at the beginning of the loading and the substrate effect.

The measured elastic moduli of the 200-, 500- and 1000-nm-thick gold films are 68.0, 69.2, and 82.5 GPa, respectively. These values are much larger than those from the strip bending tests. This is due to the fact that the strip bending test measures the modulus in the film length direction whereas the nanoindentation test, in the film surface normal direction. Since the modulus of single crystal gold is known to be dependent on the crystallographic orientation (*e.g.*, $E_{<111>}$ = 117 GPa and $E_{<100>}$ = 43 GPa), the modulus measured by the strip bending and nanoindentation tests is possibly different according to the preferential

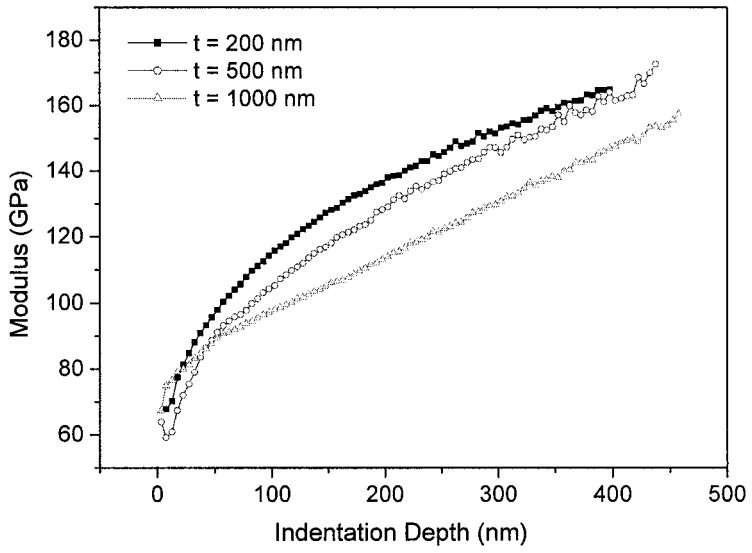

Fig. 6. Averaged elastic modulus of gold thin films as a function of the indentation depth measured by nanoindentation with a CMS option.

orientation in each direction. According to the work of Espinosa *et al.*,[5] e-beam-evaporated gold films exhibited a strong <111> texture in the surface normal direction. With this dominant <111> texture, nanoindentation will give a much higher elastic modulus than the strip bending test. This explanation cannot certainly be applied directly to the analysis of our results because the deposition method and process conditions are totally different. Further investigation and analysis on the film texture of our specimens will be required to explain the lower modulus.

It is interesting that the elastic modulus for the1000-nm-thick gold films is larger than those of the other films. According to this result and the above discussion about the film texture, we can expect that the modulus for the 1000-nm-thick films measured by the strip bending test will be smaller than those of the other films. Unfortunately, the modulus values from the strip bending test are almost similar regardless of the specimen thickness, as shown in Table 1. This experimental mismatch is believed to be due to several reasons: the errors of the nanoindentation data in a very small-depth region below 50 nm, significant buckling behaviors of the 1000-nm-thick films, and experimental errors such as a misalignment of the indenter tip.

4. Conclusions

Mechanical properties of nanometer-thin gold films were measured using strip bending and nanoindentation tests for MEMS/NEMS applications. Concepts and experimental methodologies of the strip bending test were established. Freestanding gold strip specimens were fabricated by micromachining technology with careful considerations about the mechanical design and the effect of the process. Strip specimens with different thicknesses were tested by the constructed strip bending technique to reveal the size effect on the mechanical properties. Elastic modulus was measured in a range of 27–37 GPa with no notable dependence on the film thickness. However, the plastic deformation and strength of the film exhibited obvious dependences on the film thickness. The initial stress existing in the released film changed from tension to compression as the film thickness increased. Increased yield and tensile stress with decreasing thickness clearly showed brittle behaviors of thinner films. The nanoindentation test gave a much higher elastic modulus than the strip bending test. Further investigations about the film texture and the methods of reducing measurement errors are required to enhance the accuracy of both techniques.

It was demonstrated that the strip bending test could provide some repeatable results on the working specimens. The strip bending test will be useful in evaluating the mechanical characteristics of micro-nano-scale structures along with the conventional nanoindentation test.

Acknowledgements

This research was supported by a grant (03K 1401-01230) from the Center for Nanoscale Mechatronics & Manufacturing of the 21st Century Frontier Research Program.

References

1 X. Li, B. Bhushan, K. Takashima, C. W. Baek and Y.K. Kim: Ultramicroscopy **97** (2003) 481.
2 N. Namazu, Y. Isono and T. Tanaka: J. Microelectromech. Syst. **9** (2000) 450.
3 H. D. Espinosa and B. C. Prorok: J. Mater. Sci. **38** (2003) 4125.
4 J. M. Kim, C. W. Baek, Y. K. Kim, P.Nardi and X. Li: The 5th Korean MEMS Conference (KIEE, Jeju, 2003) 409.
5 H. D. Espinosa, B. C. Prorok, and M. Fischer: J. Mech. Phys. Solids **51** (2003) 47.
6 T. P. Weihs, S. Hong, J. C. Bravman and W. D. Nix: J. Mater. Res. **3** (1998) 931.
7 W. N. Sharpe, J. Bin Yuan and R. L. Edwards: J. Microelectromech. Syst. **6** (1997) 193.
8 C. W. Baek, Y. K. Kim, Y. Ahn and Y. H. Kim: Sensors and Actuators A **117** (2005) 17.
9 W. C. Oliver and G. M. Pharr: J. Mater. Res. **7** (1992) 1564.